Journal of Physics B:
Atomic, Molecular and
Optical Physics

Orientational anisotropy of photoemitting CS_2 molecules induced by molecular field splitting

OPEN ACCESS
IOP Publishing
Journal of Physics B: Atomic, Molecular and Optical Physics
J. Phys. B: At. Mol. Opt. Phys. **58** (2025) 205101 (11pp)
https://doi.org/10.1088/1361-6455/ae0a97

Orientational anisotropy of photoemitting CS_2 molecules induced by molecular field splitting

E Kukk[1,*], J Niskanen[1], L Pihlava[1], S Granroth[1], M Berholts[2], O H Hafiani[3] and C Stråhlman[4]

[1] Department of Physics and Astronomy, University of Turku, FI-20014 Turku, Finland
[2] Institute of Physics, University of Tartu, W. Ostwaldi 1, EE-50411 Tartu, Estonia
[3] Department of Physics and Astronomy, Uppsala University, 75105 Uppsala, Sweden
[4] Department of Materials Science and Applied Mathematics, Malmö University, SE-20506 Malmö, Sweden

E-mail: edwin.kukk@utu.fi

Received 11 April 2025, revised 13 August 2025
Accepted for publication 22 September 2025
Published 16 October 2025

Abstract

We recorded the sulfur $2p$ photoelectron spectrum from gas-phase CS_2 molecules, in coincidence with the ionic fragments S^+, S^{2+} and CS^+. The fragments are created by the dissociation of the parent molecular dication following the Auger decay of the S $2p$ vacancy. The S $2p$ photoelectrons were recorded in the direction of the polarization vector of synchrotron radiation at FinEstBeAMS beamline of MAX IV synchrotron, using a hemispherical energy analyzer with sufficiently high resolution to resolve the molecular field splitting effects. The coincident ionic fragments of the linear molecule provided the orientation of the molecular axis of molecules emitting electrons in the polarization direction along the polarization vector of the incident photon beam and we obtained the orientation distributions of these molecules for photoemission from the three spin–orbit and molecular field split components in the S $2p$ orbital. The molecular field splitting introduced clear differences in the measured orientation distributions. Photoemission along the polarization vector from the $2p$ orbital with $j = {}^1/_2, m_j = \pm{}^1/_2$ created the most isotropic distribution of the emitter molecules, while the distribution corresponding to the $2p$ orbital with $j = {}^3/_2, m_j = \pm{}^3/_2$ was preferredly perpendicular to the polarization vector. Emission from the $2p$ orbital with $j = {}^3/_2, m_j = \pm{}^1/_2$ came from molecules preferably oriented along the polarization vector. We compare these results to previous theoretical predictions with a good quantitative agreement for the components with $m_j = \pm{}^1/_2$. However, the measured anisotropy for the components with $m_j = \pm{}^3/_2$ is somewhat weaker than predicted. This work demonstrates how the electron-ion coincidence technique allows, with high electron energy resolution, for testing photoelectron

* Author to whom any correspondence should be addressed.

angular distribution predictions, with the constraint that the polarization vector of the incident photons is parallel to the momentum vector of the photoelectron.

Keywords: molecular photoemission, photoionization, molecular field splitting, photoemission anisotropy, molecular orientation, photoelectron-photoion coincidence, PEPICO

1. Introduction

Characterizing the angular distribution of photoemission in the *molecular frame* of reference has long been a fruitful topic, requiring both advanced experimental techniques and careful theoretical analysis [1–6]. Various types of related information can be gathered in noncoincident experiments, such as obtaining the photoelectron angular distribution in the *laboratory frame* with the molecular orientation unknown; or obtaining the orientations of the electron-emitting molecules with the electron emission direction unknown [7, 8]. When using linearly polarized synchrotron radiation, the polarization axis fixes the orientation of the laboratory frame of reference. Coincidence measurements allow gathering information in the molecular frame, relying on the *axial recoil approximation* [2, 9–14]. Also in that case the configuration of the coincidence experiment determines the exact type of information obtained.

The most general distinction between the molecular and atomic inner-shell photoemission arises from the lowered symmetry of the system. In the case of linear molecules, cylindrical symmetry replaces the spherical symmetry of isolated atoms, reducing degeneracies of energy levels and significantly altering the observable physical quantities associated with them. In the case of 2*p* photoemission of the 3rd-row elements (Si–Cl) in small molecules, a well-known example is the degeneracy removal of the 2*p* atomic orbital due to the nonspherical symmetry—the molecular field (**MF**) splitting [7, 15–25]. The individual MF-split components of the 2*p* orbital have their specific orientation in the molecular frame, which in turn introduces characteristic properties in the angular distribution of the 2*p* photoelectrons—if these components can be resolved. When the spin–orbit (**s–o**) splitting is not negligible, its joint treatment with the MF splitting is necessary, which complicates theoretical treatment somewhat [18].

In an earlier work, we studied the high-kinetic-energy S 2*p* photoemission from CS_2, where the photoelectron recoil is seen as rotational and vibrational excitations [25]. These excitations and the related line profile depend on the orientation of the molecule receiving the recoil. Therefore, the theoretical part of the work dealt with the angular distribution of the photoelectron in the molecular frame. However, for the theoretical predictions to be comparable with the experiment, the conditions have to be defined precisely. For example, in [25], we studied the case where the photoelectron was emitted along the polarization vector of the incident radiation. Momenta of the dissociating ions were used to determine the direction of the molecular axis of the molecules that emitted electrons along the polarization vector.

Theory predicted quantitatively molecular orientations for the MF and s–o split components in the S 2*p* photoemission, which were then used to calculate the strength of recoil-excited rotations and vibrations [25]. Experimentally, the MF splitting of the 2*p* photoelectron lines in molecules containing Si, P, S, and Cl is quite small and the vibrational progressions and the lifetime and instrumental broadening profiles overlap [22]. Especially in high-kinetic-energy measurements, reducing the instrumental contribution sufficiently to resolve the MF-split components poses a challenge [25]. In this work, we focus on the near-threshold S 2*p* photoemission, where the recoil effects are negligible. Under these low-kinetic-energy conditions, we can resolve the MF-split components in the photoelectron spectrum, coincident with fragment ions, and determine the molecular orientation distributions. However, while fast electrons are insensitive to alterations of the scattering potential, it remains an open question how well a simple atomic model describes the process when a slow photoelectron experiences a molecular potential strongly deviant from the spherical atomic one. In the used experimental scheme (figure 1), we obtain the orientation distributions of the molecules emitting photoelectrons along the polarization vector. This is equivalent to obtaining the molecular-frame photoelectron angular distribution, but **only** for the subset of electrons that are emitted along the polarization vector $\hat{e}$.

Below, we report the experimental results and compare them with the theoretical predictions from [25].

2. Experiment

The experiment was performed at the Finnish–Estonian beamline (FinEstBeAMS) of the MAX IV synchrotron radiation source in Lund, Sweden, using the gas-phase coincidence end-station GPES [26]. The beamline [27, 28] is equipped with a SX700 type monochromator manufactured by FMB Feinwerk-und Messtechnik GmbH, receiving radiation from an Apple II type undulator. Horizontally polarized radiation was used in this experiment.

Carbon disulfide (CS_2, Merck, purity $\geqslant$99%) molecules were introduced by direct evaporation from a liquid reservoir at room temperature, after purifying by two freeze-thaw cycles. The molecular beam crossed the monochromatized photon beam at the centre of the sample region (figure 1). Photoelectrons were detected by a modified Scienta R4000 hemispherical electron analyzer, equipped with a fast

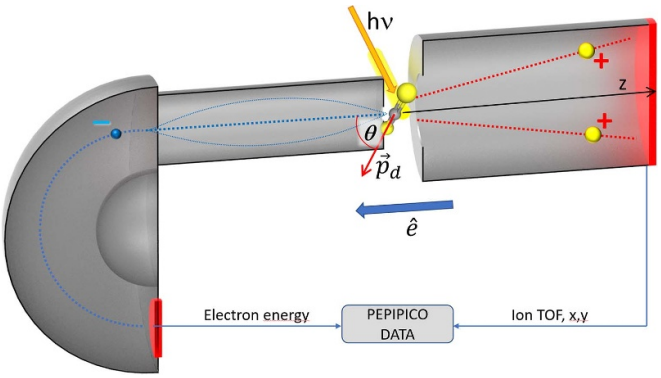

Figure 1. Experimental scheme of the PEPIPICO measurements at the FINEstBeams beamline of MAX IV. The photon beam ($h\nu$) is perpendicular to the axis of the ion spectrometer and electron lens, and the polarization vector $\hat{e}$ is along that axis. The vector $\vec{p}_{\rm d}$ is obtained as the difference of the momenta of two ionic fragments and represents the direction of the molecular axis.

40 mm diameter microchannel plate (MCP) and a resistive anode (Quantar Inc.) position-sensitive detector. The electron detector provided triggers for the pulsed ion extraction voltage of 600 V across the source region of a modified Wiley–McLaren type ion time-of-flight (TOF) spectrometer [26]. The ions were then accelerated to the final energy by the drift tube potential of −1850 V, first passing a 'lens' aperture at −250 V potential, modifying the radial distribution and focusing. Ions were detected by a Roentdek 80 mm diameter MCP and HEX-anode detector, recording ion flight times and hit positions on the plane perpendicular to the spectrometer's axis. Electron energy, ion TOFs, and hit positions were combined into a coincidence dataset. In addition, non-coincident 'random' triggers for ion extraction were generated at a constant rate, interleaved with the 'true coincidence' electron triggers. The ions collected using the random triggers were used for statistical subtraction of the false coincidence background from the ion TOF spectra, electron-ion-ion coincidence maps, coincident ion pair yields, and ion momentum distributions.

The electron energy window of about 4 eV for a coincidence dataset was defined by the pass energy $E_{\rm p} = 50$ eV of the analyzer. Electron energy resolution was set to about 105 meV and the photon bandwidth to 30 meV at the photon energy of 200 eV. Under these conditions, the coincident electron count rate was 20–25 $\rm s^{-1}$. As an indication of ion count rates, 45% of these electron triggers produced ion pairs in the TOF range of interest (figure 3 of section 3.2), while 8.4% of the random triggers produced such ion pairs.

3. Sulfur 2p photoionization and molecular dissociation

3.1. S 2p photoelectron spectrum

Photoemission from the sulfur 2p orbital has been studied by noncoincident electron spectroscopy in several sulfur-containing molecules [7, 8, 17, 18, 21, 22, 24, 25, 29–32]. In general, the spectral structure is defined by three main factors: (i) s–o splitting of the 2p energy level to two sub-levels with different one-electron total quantum number j, (ii) vibrational excitations due to the change of bond length upon ionization, mainly of the asymmetric stretching normal mode [22], and (iii) the MF splitting. The latter appears since atomic one-electron wavefunctions, characterized by the j and m_j quantum numbers after the s–o coupling, experience different molecular potentials due to their different orientation. MF splitting only appears when the symmetry of the molecule is low enough so that the three atomic 2p wavefunctions form the bases of different irreducible representations—in all linear molecules, for example. In the present case of CS_2, MF separates energetically the $2p\ j = {}^3/_2, |m_j| = {}^1/_2$ and $j = {}^3/_2, |m_j| = {}^3/_2$ wavefunctions (abbreviated from here on as $2p_{{}^3/_2{}^1/_2}$ and $2p_{{}^3/_2{}^3/_2}$), that in a free atom correspond to the degenerate $2p_{{}^3/_2}$ s–o component.

Here we use the atomic j, m_j notation throughout as consistent with the applied atomistic model that neglects interatomic orbital interaction. However, the inner-shell p orbitals are often described in terms of the symmetry of the MF, i.e. in linear molecules using th σ and π notation [24]. They correspond to the quantum numbers $|m_l| = 0$ and 1, correspondingly. It therefore follows that the $2p_{{}^3/_2{}^3/_2}$ component (that can only arise when $|m_l| = 1$) is of pure π character, while the other two are of mixed σ–π character.

Figure 2 shows the S 2p photoelectron spectrum of CS_2, measured about 30 eV above the S 2p ionization threshold. The two main resolved structures correspond to the atomic s–o splitting, but in order to resolve any additional features, a least-squares curve fitting was carried out. The result of the fitting is shown as three colored lines, with the black curve through the data points as their sum. The three colors correspond to the three atomic wavefunctions $2p_{j|m_j|}$. Each of the three curves shows an additional structure due to vibrational excitations. In the fitting, these vibrational envelopes were required to have the same structure (spacing and relative intensities); all individual peaks were also required to have equal lifetime width and instrumental broadening. The relative binding energies of

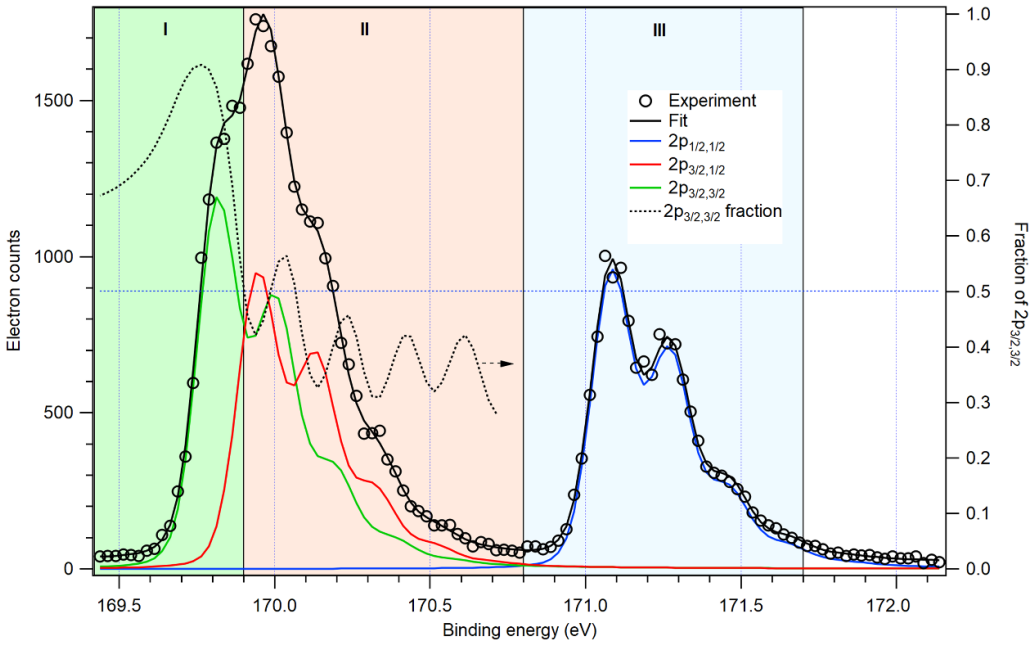

Figure 2. Sulfur 2p photoelectron spectrum from CS_2, measured at 200 eV photon energy, showing the experimental data points (circles) with a fitted curve (black line), which is decomposed into three s–o and MF-split component (coloured curves). The dotted black line with the right-hand scale shows the fraction of the $2p_{3/2}{}^3{}_{/2}$ component's intensity from total. The three regions I–III are colored according to the dominant component of $2p$ and were used to extract the orientation distributions of the three components in the photoelectron spectrum.

the three components, as obtained from the fit, are:

$$E_\mathrm{b}\left(2p_{3/2}{}^3{}_{/2}\right) = 0\,\mathrm{ev},$$
$$E_\mathrm{b}\left(2p_{3/2}1_{/2}\right) = 0.129(5)\,\mathrm{ev},$$
$$E_\mathrm{b}\left(2p_{1/2}1_{/2}\right) = 1.268(5)\,\mathrm{ev}.$$

A single value of the common vibrational spacing was obtained as 190(5) meV, very close to 19 eV that was assigned to the asymmetric stretching by Wang *et al* [22]. Fitted Lorentzian width was 49(13) meV and Gaussian broadening 155(10) meV.

Since the two $2p_{3/2|m_j|}$ components are not completely separated in energy, electron-energy-filtered observed quantities will necessarily be of a mixed character, dominated by either of the components depending on the electron energy. In order to quantify this mixing and extract the characteristics of the 'pure' MF-split components, we derived first the ratio of the two MF-split components, $2p_{3/2}{}^3{}_{/2}$ to $2p_{3/2}1_{/2}$, from the fit. It is given by the black dotted line in figure 2 and shows, for example, how the low-energy shoulder of the $2p_{3/2}$ structure is dominated by the $2p_{3/2}{}^3{}_{/2}$ component.

3.2. Molecular dissociation

Inner-shell photoionization is predominantly followed in a few femtoseconds by nonradiative Auger decay, creating a molecular dication and leading with high probability to the dissociation of the molecule. These processes, the fragmentation pathways and dynamics has been studied before [33–35]; below we summarize the present results as the material from which the fragment momenta and, eventually, the molecular orientations were derived. The overall characteristics of the molecular dynamics following S $2p$ inner-shell ionization and Auger decay are given by the photoelectron–photoion–photoion (PEPIPICO) map of figure 3. The three possible fragmentation pathways of the doubly charged parent ion that yield singly charged fragments pairs—(S_a^+, CS_b^+),(S_a^+, S_b^+, C) and (C^+, S_a^+, S_b)—have approximately equal probability (each $\approx 1/3$ of the pair count). For clarity, we will denote the two S atoms or ions in the fragment pairs by indexes a and b. These PEPIPICO patterns are accompanied by 'shadows' due to the less abundant ^{34}S isotope. There are also much weaker patterns involving doubly charged ions from the dissociation of CS_2^{3+}, that can be produced for example by shake-off transitions. They constitute about 12% of the total number of coincident ion pairs.

4. Molecular orientation in S 2p photoemission

4.1. Experimental results from ion momenta

One of the main dissociation channels of ${CS_2}^{2+}$ is $S_a^+ + S_b^+ + C$. Assuming the simplest model case of concerted dissociation where the neutral particle gets no momentum, there is no thermal motion and no rovibrational excitation occur, the

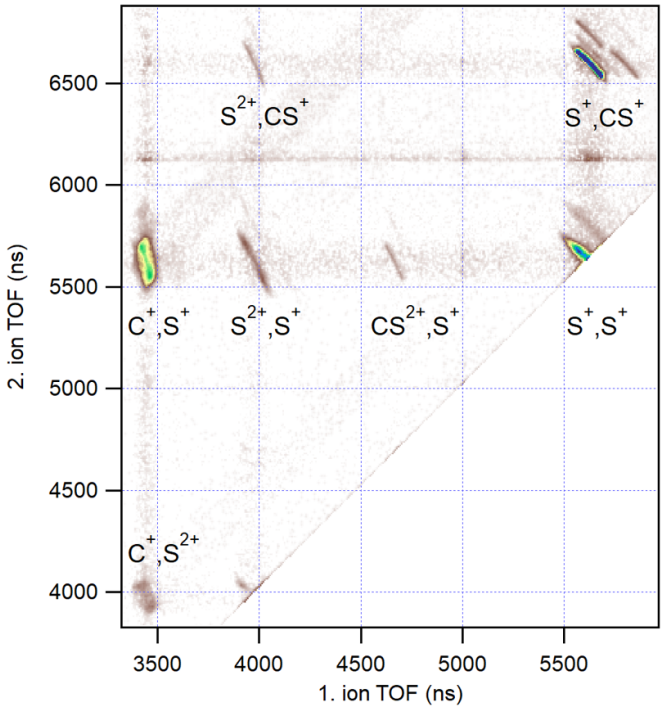

Figure 3. Photoelectron–photoion–photoion map of the fragmentation products of CS_2^{2+}, detected together with the S 2*p* photoelectron. The ion pairs are plotted against the time-of-flight of the first (faster) and second (slower) ion. The strongest patterns are labeled by the corresponding ion pairs.

momenta of sulfur ions are directed along the molecular axis. In principle, the momentum of either of the ions is sufficient to define the molecular axis, but in our experiment, this directional information is more accurately conveyed by their *difference* (see figure 1):

$$\vec{p}_{\mathrm{d}} = \vec{p}_{Sa} - \vec{p}_{Sb}. \tag{1}$$

For example, effects of the experimental spread in the initial x, y, z position of the dissociating molecule (the finite source region size), and of the translational thermal motion of the parent molecule, will cancel out in the $\vec{p}_{\mathrm{d}}$ quantity.

We will present the results regarding the orientation distributions of $\vec{p}_{\mathrm{d}}$, for the different MF- and s–o split components in the 2*p* photoemission. We analyzed three ion pair patterns in the PIPICO map, for which the axial recoil approximation is a reasonable assumption: (S_a^+,S_b^+), (S_a^+, CS_b^+), and (S_a^+, S_b^{2+}), the latter having a much poorer statistics.

After extracting the coincident ion pairs, associated with each of the three photoelectron energy ranges shown in figure 2, the distribution histograms of $\vec{p}_{\mathrm{d}}$ were generated. The highest-binding-energy region III corresponds directly to the $2p_{1/2}1/2$ component. For the two components $2p_{3/2|m_j|}$, the extracted distributions for regions I and II are mixtures from the two. The fraction of $2p_{3/2}{}^{3}/_{2}$ is 0.816 in region I and 0.452 in region II, according to the dotted curve of figure 2. Using these values, it was possible to convert the extracted orientation distributions of regions I and II to the 'pure' $2p_{3/2}{}^{3}/_{2}$ and $2p_{3/2}1/2$ distributions. These are shown in figures 4(a) and (b) for the first two ion pair patterns of good statistics. The curves correspond to the three 'pure' s–o and MF components and are color-coded as in figure 2.

The experimental distributions in figures 4(a) and (b) were fitted with a distribution function

$$p(\theta) = I\left[A\sin^2\theta + (1-A)\cos^2\theta\right], \tag{2}$$

where θ is defined as the angle between the vector $\vec{p}_{\mathrm{d}}$ and the axis of the ion spectrometer, which is collinear with the polarization direction, and the emission direction of of the detected electron (figure 1). I is the total intensity scaling factor and the deviation of the coefficient A from 0.5 gives the degree of anisotropy of the distribution.

Before reporting the results of these fits, let us consider the instrumental errors and other similar sources of broadening that are present in the determination of $\vec{p}_{\mathrm{d}}$. In particular, we investigate whether these random errors introduce a systematic bias in the experimentally determined coefficients A in equation (2). These considerations are presented in detail in appendix and are summarized in table 1. Briefly, both the instrumental error in determining the individual momenta, and the deviations from the antiparallelism of the two momenta due to deviations from the axial recoil approximation, are seen in the angle γ *between* the two momenta. These deviations $\Delta\gamma$ are used to estimate the error $\Delta\theta$ for the direction of $\vec{p}_{\mathrm{d}}$. A Gaussian random error in determining the angle θ smears out the angular distributions by convolution and brings the coefficients A close to the isotropic value of 0.5. The inverse correction (essentially deconvoluting the distributions) was applied to the fitted values of A.

Table 1. Data analysis results from coincident ion pairs. The table contains: (1) Correlation of the momentum vectors of the charged fragments, (2) rotational effects on the momenta, (3) total angular broadening, (4) fitting coefficients A of equation (2) to the $p_{\rm d}(\theta)$ distributions for the three $p_{j|m_j|}$ components, and (5) the coefficients A after isotropic renormalization of the combined distribution. Errors in brackets represent only the statistical uncertainty of the least-squares fitting.

	Quantity	(S_a^+,S_b^+)	(S_a^+,CS_b^+)	(S_a^+,S_b^{2+})
1	Deviation from $\cos\gamma=-1$			
	$\Delta(\cos\gamma)$	0.108	0.017	0.104
	$\Delta\theta$	27°	9°	25°
2	Average thermal rotation angle of $p_{\rm d}$			
	$\Delta\theta_{rot}$	8.2°	5.5°	5.9°
3	Total broadening of $p_{\rm d}$ orientation			
	FWHM	33°	19°	30°
4	Fitted A coefficients			
	$A(2p_{3/2\,3/2})$	0.580(24)	0.570(18)	0.67(10)
	$A(2p_{3/2\,1/2})$	0.225(28)	0.363(23)	0.46(12)
	$A(2p_{1/2\,1/2})$	0.356(10)	0.416(9)	0.44(4)
5	Fitted A coefficients, isotropic renorm.			
	$A(2p_{3/2\,3/2})$	0.711(24)	0.625(18)	0.65(10)
	$A(2p_{3/2\,1/2})$	0.344(28)	0.418(23)	0.44(12)
	$A(2p_{1/2\,1/2})$	0.488(10)	0.471(9)	0.43(4)

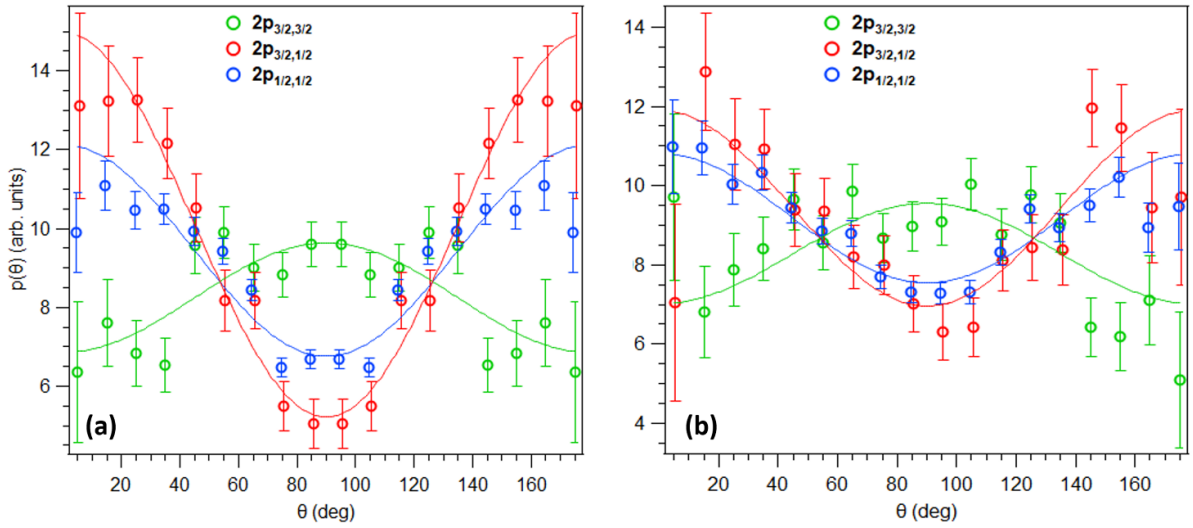

Figure 4. Orientation distributions of the CS_2 molecules emitting the three s–o and MF split components of the S 2p photoelectrons in the polarization direction. Experimental data points are given by circles; continuous lines are least-squares fits of equation (2). Graphs (a) and (b) are extracted from the (S_a^+, S_b^+) and (S_a^+, CS_b^+) pairs, respectively. All distributions are divided by the $\sin\theta$ geometrical factor for better visualization. Original data spans the range from 0 to 90° in graph (a) and is reflected to 90°–180° for better visualization.

The results of fitting the experimental orientation distributions with equation (2) are reported in table 1, after performing the above corrections: converting to the 'pure' $2p_{3/2}{}^3/_2$ and $2p_{3/2}1/_2$ distributions and removing the anisotropy-reducing effect of the instrumental and thermal broadening.

Qualitatively, all ion pairs give a very similar result: the $2p_{3/2}{}^3/_2$ electrons, emitted along the polarization axis, are preferentially emitted by molecules oriented perpendicularly to that direction (see also figure 5). Conversely, the $2p_{3/2}1/_2$ electrons are preferentially emitted by molecules that were oriented along the polarization axis. For the $2p_{1/2}1/_2$ component, the observed orientational anisotropy is the weakest, also with the preferred direction along the polarization axis.

Next, the theoretical method of predicting the molecular orientation distributions is summarized and the results are compared with the experiment, followed by the analysis of possible sources of discrepancies.

4.2. Theoretical predictions

The $2p$ orbitals of the sulfur atom in a molecule are subject to two splitting mechanisms: the s–o interaction and the MF. We have previously treated the joint effect of the according

parametrized interaction Hamiltonians in the basis of the six product states $|1m\rangle\left|\frac{1}{2}m_s\right\rangle$ ($m=-1,0,1$; $m_s=-1/2,1/2$) [25]. While the s–o interaction Hamiltonian is independent of the coordinate system, the MF Hamiltonian is naturally not. In the used simple atom-in-a-molecule model, this modifies the angular distribution of the resulting lines to deviate from the s–o–split atomic case as a function of θ, the angle in between the molecular axis and the $2p$ photoelectron momentum. In the present case, there is an additional constraint that the electron momentum is parallel to the polarization of the incoming photon beam. Note that in the experimental analysis, the angle θ was defined in the laboratory frame, as that between the axis of the ion spectrometer and $\vec{p}_\mathrm{d}$. With the axial recoil approximation and the assumptions that the light is 100% polarized and the coincident electron detection is strictly limited to the polarization direction, these two definitions of θ become equivalent.

In the model, the relative photoemission cross-section $\sigma_i^{\mathrm{rel}}(R)$ for state i was derived [25] to read

$$\sigma_i^{\mathrm{rel}}(R)=\sum_{m_s}\left|\sum_m D_{0m}^{(1)}(R)\,c_{mm_s}^{(i)}\right|^2, \tag{3}$$

where $D^{(1)}(R)$ is the Wigner rotation matrix for the rotation R that transforms the laboratory frame to the molecular one, and $c_{mm_s}^{(i)}$ are the expansion coefficients of the eigenstate i in the aforementioned product basis in the molecular frame of reference.

We use the coefficients $c_{mm_s}^{(i)}$ of [25] for the combined effect of the s–o and MF Hamiltonians. For comparison with experiment, the angular distribution functions for the three doubly degenerate components read

$$\begin{aligned}
\sigma^{\mathrm{rel}}_{^3/_2{}^3/_2} &= 0.500\left(1.000\sin^2\theta\right),\\
\sigma^{\mathrm{rel}}_{^3/_2{}^1/_2} &= 0.793\left(0.261\sin^2\theta+0.739\cos^2\theta\right),\\
\sigma^{\mathrm{rel}}_{^1/_2{}^1/_2} &= 0.707\left(0.414\sin^2\theta+0.586\cos^2\theta\right),
\end{aligned} \tag{4}$$

when the form of equation (2) and table 1 is used. We note that these functions do not account for the varying probability of observing a molecular orientation with the angle θ in the randomly oriented sample, which follows an additional geometric factor $\sin\theta$. One can also relate the coefficients A to the symmetry character of the three components in equation (4): the $2p_{^3/_2{}^3/_2}$ component of purely π symmetry has $A=1$.

5. Discussion

Qualitatively, the experiment and theory are in agreement for all three MF- and s–o split components: the $2p_{^3/_2{}^3/_2}$ component's distribution, for example, has the dominant contribution from the molecules aligned perpendicular to the electron emission direction along the polarization vector. Quantitatively, however, the agreement is not complete—the model predicts that for the $2p_{^3/_2{}^3/_2}$ component, the contribution from molecules aligned parallel to the electron detection direction drops to zero ($A=1$), whereas the experiment gives $A=0.58$ for (S_a^+,S_b^+) and 0.57 for (S_a^+,CS_b^+).

When adding up all three distributions (i.e. obtaining molecular orientation for the total $2p$ photoemission), one notices that the combined distribution remains clearly anisotropic, with the perpendicular orientation depressed. On the one hand, this depression can be an instrumental artifact due to an increased possibility of ion loss for the strongly non-axial trajectories (see, e.g. [36]). In addition, in the case of the (S_a^+,S_b^+) pair the two sulfur ions, emitted from a molecule with an axis perpendicular to the TOF axis have nearly equal flight times, which can result in reduced detection efficiency.

On the other hand, the isotropic orientation of all three components combined would be the baseline theoretical assumption when the inner-shell photoemission is taken as entirely atomic with the only effect of the MF being the removal of the degeneracy of the $2p$ wavefunctions. We therefore added part 5 to table 1, where the obtained distributions were renormalized to give the combined isotropic distribution and correcting for possible instrumental anisotropy.

The summary of the original and the isotropically renormalized fitting coefficients A is given in figure 5, presenting also the theoretical values. In addition, a polar plot of figure 6 shows the theoretical and experimental distribution curves for the (S^+,S^+) pairs, with both the original and normalized A coefficients.

The (S_a^+, S_b^+) and (S_a^+, S_b^{2+}) fragments are released in a three-body process, in which the third, neutral particle can in principle seriously disturb the axial recoil approximation. One notes that if the dissociation geometry has inversion symmetry at all stages, the direction of the vector $\vec{p}_\mathrm{d}$ is not affected by any momentum transfer to the C atom. However, the neutral C fragment obtaining a significant fraction of the momentum release in a symmetric, concerted dissociation would be seen in the PIPICO map due to the change of the angle γ between the two momenta. Indeed, the deviation for $\cos\gamma$ is clearly larger fo the (S_a^+,S_b^+) pair than for the two-body dissociation pair (S_a^+, CS_b^+) (table 1, part 1).

As an alternative to a concerted dissociation, a two-step process of secondary dissociation creates first the $S_a^+ + CS_b^+$ fragments and, after a (considerable) delay, the CS_b^+ separates into the S_b^+ and C fragments. The secondary dissociation process can destroy the recoil approximation, if a large part of the momentum is released in the second, neutral fragment separation step. This is, however, unlikely.

The main experimental signature of the secondary dissociation is an altered division of the magnitude of the momenta—since initially the momentum of the Coulomb explosion is received by the CS_b^+ fragment, the final ratio $|p_{S_b}|/|p_{S_a}|$ is not 1.0 as for a concerted dissociation, but 32/44 = 0.73. Investigation of $|p_{S_b}|/|p_{S_a}|$ showed a distribution centered at ratio 1.0, however. Secondary dissociation would also be seen in the slope of the (S_a^+,S_b^+) pattern of the PIPICO map, changing from $-45°$ to both $-36°$ and $-54°$ at the asymptotic limit of secondary dissociation. Analysis of the experimental data gives the slope of the pattern as $-45.05(4)°$ with no indication of pattern splitting and slope change that would indicate

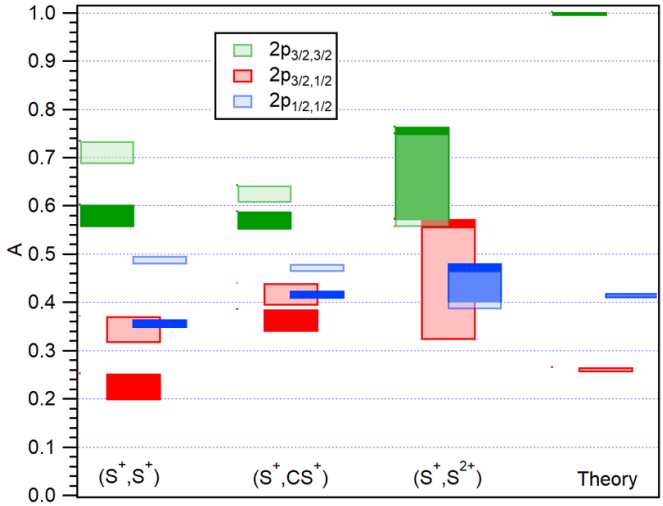

Figure 5. Summary of the analysis of orientation distributions for three ion pairs: coefficients A from table 1. Solid-colored bars are the original fitting results from Part 4 of table 1 and the shaded bars are isotropically renormalized (Part 5). The height of the bars corresponds to the standard errors from least-squares fitting. Theoretical values are given in the last column.

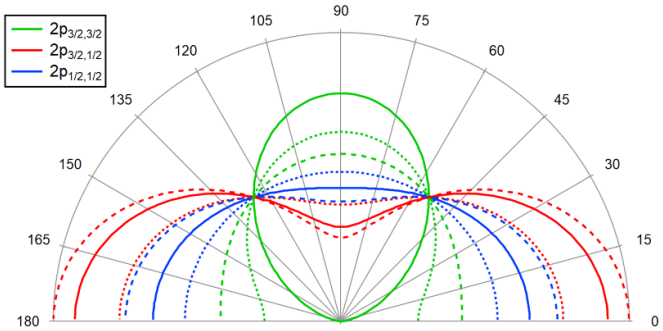

Figure 6. Comparison of the theoretically predicted orientation distributions (solid lines) with the experimental results from the (S^+,S^+) ion pair (dashed lines: original result, dotted lines: isotropically renormalized). The angle $\theta = 0$ corresponds to the direction of both the electron emission and the polarization vector. The curves do not include the geometrical $\sin\theta$-factor.

a secondary dissociation process. The pattern is broader than the two-body (S_a^+,CS_b^+) pattern, which, although attributable to the neutral carbon receiving some momentum in instantaneous dissociation, could also be due to the slightly delayed CS^+ fragment dissociation.

Multi-body dissociation obviously cannot account for the reduced $2p_{3/2}{}^3{}_{/2}$ anisotropy when derived from the two-body (S_a^+,CS_b^+) pattern and yet, the experimental results do not show any stronger anisotropy in this case (figure 5 and table 1). We therefore conclude that multi-body effects and the resultant blurring of the axial recoil approximation are not the principal cause of the quantitative differences between the experiment and the theory, although they could slightly influence the results obtained from the (S_a^+,S_b^+) pattern.

Lastly, from the theoretical point of view, the calculated anisotropies arise when considering the degeneracy-removing effect of the MF on the bound atomic inner-shell orbitals. The effect of MF on the outgoing continuum waves was not accounted for and could be a factor altering the predicted distributions, e.g. reducing the anisotropy of the $2p_{3/2}{}^3{}_{/2}$.

6. Conclusion

The electron-energy-resolved PEPIPICO technique was successfully used to extract molecular-frame angular information on the S $2p$ photoemission of the individual MF and spin–orbit split components. The high electron energy resolution of the hemispherical analyzer allowed us to resolve the minor MF splitting in the photoelectron spectrum, combined with reliable determination of the molecular axis orientation by the 3D momentum-resolving multi-ion detection. Comparison with the effective atomic model reveals an good match for the $2p_{1/2}{}^1{}_{/2}$ and $2p_{3/2}{}^1{}_{/2}$ components, whereas for the $2p_{3/2}{}^3{}_{/2}$ isolated component, the experiment shows weaker anisotropy than predicted, although both are still in qualitative agreement. We have considered various experimental sources for the discrepancy, and corrected for instrumental effects.

The simple model used in this work can be improved, *e.g.*, by accounting for the molecular-geometry-induced effects on the departing photoelectron, such as intramolecular scattering. The used experimental technique allows for testing such more advanced photoelectron angular distribution predictions, when

evaluated with the constraint that the polarization vector of the incident photons is parallel to the momentum vector of the photoelectron.

Data availability statement

All data that support the findings of this study are included within the article (and any supplementary files).

Acknowledgments

We thank Antti Kivimäki, Kirill Chernenko and other MAX-IV staff for their generous help during the beamtime. MB acknowledges financial support from the Estonian Research Council (Grant PSG1037) as well as support from the Estonian Ministry of Education and Research (TK210, Centre of Excellence in Sustainable Green Hydrogen and Energy Technologies). OHH acknowledges support from the Swedish Research Council (Grant 2018-00740) and from the PRISMAS Project, funded under the Horizon Europe Research and Innovation programme, Marie Skłodowska-Curie Actions (Grant 101081419).

Appendix. Statistical and systematic error analysis

Below we consider the three main sources that affect the experimentally obtained molecular orientation distributions.

Momentum resolution of the ion spectrometer: Denoting the instrumental variation of the measured orientation of the individual momentum vectors $\vec{p}_{Sa,b}$ as angle error $\Delta\alpha(\vec{p}_S)$, one can estimate the error of the orientation of $\vec{p}_\mathrm{d}$ as $\sqrt{2}\Delta\alpha(\vec{p}_S)$. This is also the error of determining the angle between the individual vectors, $\gamma = \angle(\vec{p}_{Sa},\vec{p}_{Sb})$. Making a baseline assumption that originally $\cos\gamma = -1$, an experimental deviation from this value can be studied. For the $(\vec{p}_{Sa}, \vec{p}_{Sb})$ pairs, the measured $\cos\gamma$ distribution was well described by the exponential function

$$p(\cos\gamma) = \exp\left(-\frac{1+\cos\gamma}{\delta}\right) \tag{5}$$

with $\delta = 0.108$. This also gives the experimental error for determining the orientation angle θ of $\vec{p}_\mathrm{d}$. This uncertainty affects the angular distributions that depend on θ; we found the effect to be well represented by a convolution with a Gaussian broadening with FWHM $w = 27.8°$.

In the case of the two-body channel $CS_2 \rightarrow S^+ + CS^+$, the PIPICO pattern is considerably sharper (figure 3). Analysis of the $\cos\gamma$ distribution ($\gamma = \angle(\vec{p}_{Sa},\vec{p}_{CS_b})$) in this case gives $\delta = 0.017$, corresponding to the Gaussian broadening of 8.7° FWHM for figure 4(b). Lastly, for the $(\vec{p}_{Sa^+},\vec{p}_{Sb^{++}})$ pairs, $\delta = 0.104$.

We are ultimately interested in how this broadening reduces the observed anisotropies. The instrumental effect of reducing the observed anisotropy is the strongest for $A = 0$ or 1 (equation (2) in the main text), and has no effect with the isotropic distribution of $A = 0.5$. We found a general empirical relationship between the convoluted and unconvoluted orientation distributions of $\vec{p}_\mathrm{d}$ as

$$A \approx \frac{2A_\mathrm{conv} - c}{2(1-c)}, \quad c \equiv 1.41\times10^{-3}w + 6.2\times10^{-5}w^2, \tag{6}$$

where A is the $\sin^2\theta$ coefficient in the original distribution and w[degrees] is the FWHM of the convoluting Gaussian function.

Thermal rotational and vibrational motion: The molecules in a gas-phase sample are in thermal motion, involving also the rotational and vibrational degrees of freedom. The degrees of freedom directly affecting the direction of the momenta of the dissociation products are the bending vibrations and rotations around the two rotational axes in the molecular frame.

In the case of rotations, the orientation of $\vec{p}_\mathrm{d}$ is altered. Although various ballpark estimates of this change can be made, we estimated the effect of rotations by numerical simulations of dissociating molecules (as point charges) in a thermal motion. The two rotational degrees combined have an average thermal energy of 25 meV at room temperature. At this energy, and using the S_a^+, S_b^+ ion pair for orientation determination, the change in the orientation of the $\vec{p}_\mathrm{d}$ vector is 8.4° (with the initial C–S bond length of 1.55 Å). Notably, the effect of the rotation is not visible in the angle γ between the individual vectors and is therefore not incorporated by the experimental error determination presented above. However, its effect on the orientation distributions can also be represented by a convolution with a Gaussian distribution for the rotation of the $\vec{p}_\mathrm{d}$ to a random direction, having FWHM of 13.6°. For the bending vibrations, since the motion is symmetric for the two sulfur atoms and our analysis is based on the $\vec{p}_\mathrm{d}$ vector, its direction is not affected by this motion in the case of the S_a^+, S_b^+ ion pair analysis.

An analogous analysis was done for the other two ion pairs, presented in table 1 of the main manuscript. In simulating dissociation into the (S_a^+, CS_b^+) pairs, a harmonic bond with $k = 2500\,\mathrm{N\,m^{-1}}$ was added between the C and S_b atoms and both were assigned the charge of +0.5e. In this case, the bending vibrations can also affect the molecular orientation determination, since (a) about 10% of the molecules are at the first excited vibrational level at room temperature and (b) upon dissociation, part of the vibrational energy becomes rotational motion of the two fragments. This is also represented by the classical numerical simulation where, using the thermal average energy per bending degree of freedom, only about 0.1° change in the orientation of $\vec{p}_\mathrm{d}$ is obtained. Therefore, vibrational motion is not a significant factor also in the case of the S_a^+, CS_b^+) pattern.

Photoelectron recoil: Rotational motion can also be induced by the recoil momentum of the photo- and Auger-electrons, with a similar effect on the RF-IF transition as the thermal rotations. The total recoil energy of 32 eV photoelectrons emitted from S atoms is 0.55 meV and for the Auger electrons of the average energy of 180 eV, 3.1 meV. Only a fraction of this energy is used for rotational excitations, remaining less than 10% of the thermal energy. Therefore, we conclude that in this experiment with near-threshold photoemission, the photoelectron recoil is not a significant additional factor to be considered.

Photoelectron acceptance angle: The 2*p* photoelectrons are collected from a certain solid angle by the electron analyzer, determined by its transmission. It is affected by many factors, such as the electron lens settings, pass and kinetic energies, source dimensions and alignment. The opening angle of the acceptance cone can be up to 20° according to the manufacturer's documentation, which then introduces a corresponding broadening in the determination of $\vec{p}_\mathrm{d}$ in respect to the polarization direction. As a ballpark estimate, we approximate it as a Gaussian broadening with FWHM of 10°, multiplied with a $\sin\theta$ geometrical factor.

For the final correction, all three broadenings—TOF spectrometer's, rotational and electron spectrometer's—were convoluted, giving the total FWHM as 33.3°, 19.2°, and 29.5° for the (S_a^+, S_b^+) ,(S_a^+, CS_b^+) and (S_a^+, S_b^{2+}) ion pairs, respectively. Equation (6) was then used to calculate the corrected coefficients A.

ORCID iDs

E Kukk 0000-0001-5275-5913
L Pihlava 0000-0001-7467-6968
M Berholts 0000-0001-7609-6262
O H Hafiani 0000-0002-6440-1909

References

[1] Liu X-J, Lucchese R R, Grum-Grzhimailo A N, Morishita Y, Saito N, Prümper G and Ueda K 2007 Molecular-frame photoelectron and electron-frame photoion angular distributions and their interrelation *J. Phys. B: At. Mol. Opt. Phys.* **40** 485
[2] Lucchese R R, Carey R, Elkharrat C, Houver J C and Dowek D 2008 Molecular frame and recoil frame angular distributions in dissociative photoionization of small molecules *J. Phys.: Conf. Ser.* **141** 012009
[3] Williams J B *et al* 2012 Polyatomic molecules in three dimensions using molecular frame photoelectron angular distributions *Phys. Rev. Lett.* **108** 233002
[4] Yagishita A 2015 Photoelectron angular distributions from single oriented molecules: past, present and future *J. Electron Spectrosc. Relat. Phenom.* **200** 247
[5] Ota F, Yamazaki K, Sébilleau D, Ueda K and Hatada K 2021 Theory of polarization-averaged core-level molecular-frame photoelectron angular distributions: I. A full-potential method and its application to dissociating carbon monoxide dication *J. Phys. B: At. Mol. Opt. Phys.* **54** 024003
[6] Vela-Peréz I *et al* 2023 High-energy molecular-frame photoelectron angular distributions: a molecular bond-length ruler *Phys. Chem. Chem. Phys.* **25** 13784
[7] Kukk E, Bozek J D, Sheehy J A, Langhoff P W and Berrah N 2000 Angular distribution of molecular-field-and spin-orbit-split sulfur 2p photoemission in OCS: a sensitive probe of the molecular environment *J. Phys. B: At. Mol. Opt. Phys.* **33** L51
[8] Turri G *et al* 2004 Spin- and angle-resolved spectroscopy of S2p photoionization in the hydrogen sulfide molecule *Phys. Rev. A* **70** 022515
[9] Zare R N 1967 Dissociation of H_2^+ by electron impact: calculated angular distribution *J. Chem. Phys.* **47** 204
[10] Dörner R, Mergel V, Jagutzki O, Spielberger L, Ullrich J, Moshammer R and Schmidt-Böcking H 2000 Cold target recoil ion momentum spectroscopy: a 'momentum microscope' to view atomic collision dynamics *Phys. Rep.* **330** 95
[11] Cryan J P *et al* 2012 Molecular frame Auger electron energy spectrum from N_2 *J. Phys. B: At. Mol. Opt. Phys.* **45** 055601
[12] Adachi J-i, Kazama M, Teramoto T, Miyauchi N, Mizuno T, Yamazaki M, Fujikawa T and Yagishita A 2012 C 1s photoelectron angular distributions from fixed-in-space CO molecules in the high-energy continuum ≥50 eV *J. Phys. B: At. Mol. Opt. Phys.* **45** 194007
[13] Reid K L 2012 Photoelectron angular distributions: developments in applications to isolated molecular systems *Mol. Phys.* **110** 131
[14] Fukuzawa H *et al* 2019 Probing gaseous molecular structure by molecular-frame photoelectron angular distributions *J. Chem. Phys.* **151** 104302
[15] Svensson S *et al* 1994 Observation of an anomalous decay ratio between the molecular field split levels in the S 2*p* core photoelectron and *LVV* Auger spectrum of H_2S *Phys. Rev. Lett.* **72** 3021
[16] Aksela H, Kukk E, Aksela S, Sairanen O P, Kivimaki A, Nommiste E, Ausmees A, Osborne S J and Svensson S 1995 Partial Auger decay rates of core-ionized molecular states in HCl and DCl *J. Phys. B: At. Mol. Opt. Phys.* **28** 4259
[17] Siggel M R F, Field C, Sæthre L J, Bo/rve K J and Thomas T D 1996 High resolution photoelectron spectroscopy of sulfur 2*p* electrons in H_2S, SO_2, CS_2 and OCS *J. Chem. Phys.* **105** 9035
[18] Børve K J 1996 On the calculation of molecular field splitting in S 2p photoelectron spectra *Chem. Phys. Lett.* **262** 801
[19] Gel'mukhanov F, Ågren H, Svensson S, Aksela H and Aksela S 1996 Theory of Auger spectra for molecular-field-split core levels *Phys. Rev. A* **53** 1379
[20] Ellingsen K, Saue T, Aksela H and Gropen O 1997 Clt2p–photoelectron spectrum of HCl studied by fully relativistic, self-consistent-field and configuration-interaction calculations *Phys. Rev. A* **55** 2743
[21] Giertz A, Bässler M, Björneholm O, Wang H, Feifel R, Miron C, Karlsson L, Svensson S, Børve K J and Sæthre L J 2002 High resolution C1s and S2p photoelectron spectra of thiophene *J. Chem. Phys.* **117** 7587
[22] Wang H, Bässler M, Hjelte I, Burmeister F and Karlsson L 2001 A vibrationally resolved experimental study of the sulfur L-shell photoelectron spectrum of the CS_2 molecule *J. Phys. B: At. Mol. Opt. Phys.* **34** 1745

[23] Svensson S 2005 Soft x-ray photoionization of atoms and molecules *J. Phys. B: At. Mol. Opt. Phys.* **38** S821
[24] Kosugi N and Ishida T 2000 Molecular field and spin–orbit splittings in the 2p ionization of second-row elements: a Breit–Pauli approximation applied to OCS, SO_2 and PF_3 *Chem. Phys. Lett.* **329** 138
[25] Kukk E *et al* 2024 Orientational anisotropy due to molecular field splitting in sulfur 2p photoemission from CS_2 and SF_6—theoretical treatment and application to photoelectron recoil *Phys. Chem. Chem. Phys.* **26** 21810–20
[26] Kooser K, Kivimäki A, Turunen P, Pärna R, Reisberg L, Kirm M, Valden M, Huttula M and Kukk E 2020 Gas-phase endstation of electron, ion and coincidence spectroscopies for diluted samples at the FinEstBeAMS beamline of the MAX IV 1.5 GeV storage ring *J. Synchrotron. Radiat.* **27** 1080
[27] Pärna R *et al* 2017 FinEstBeaMS—a wide-range Finnish-Estonian Beamline for Materials Science at the 1.5 GeV storage ring at the MAX IV Laboratory *Nucl. Instrum. Methods Phys. Res. A* **859** 83
[28] Chernenko K *et al* 2021 Performance and characterization of the FinEstBeAMS beamline at the MAX IV Laboratory *J. Synchrotron. Radiat.* **28** 1620
[29] Coville M and Thomas T 1995 Sulfur 2p ionization energies of H2S, OCS, SO_2 and CS_2 *J. Electron Spectrosc. Relat. Phenom.* **71** 21
[30] Gedat E, Püttner R, Domke M and Kaindl G 1998 S 2p photoexcitation spectra of SO2 at high resolution *J. Chem. Phys.* **109** 4471
[31] Carlson T A, Krause M O and Grimm F A 1982 Angle resolved photoelectron spectroscopy of CS2 and COS measured as a function of photon energy from 21 to 70 eV *J. Chem. Phys.* **77** 1701
[32] Carlson T A and McGuire G 1972 Angular distribution of the photoelectron spectrum of CO_2, COS, CS_2, N_2O, H_2O and H_2S *J. Electron Spectrosc. Relat. Phenom.* **1** 209
[33] Hayes R G and Eberhardt W 1991 Electron–ion coincidences studies of the fragmentation of thiophene and of tetrahydrothiophene upon core ionization *J. Chem. Phys.* **94** 397
[34] Alkemper U and Von Busch F 1998 Auger and electron/double-ion coincidence spectroscopy of sulfur(2p)-ionized CS_2 molecules *J. Electron Spectrosc. Relat. Phenom.* **93** 115
[35] Field T A and Eland J H 1999 The fragmentation dynamics of CS_2^{2+} *Chem. Phys. Lett.* **303** 144
[36] Pihlava L *et al* 2024 Shell-dependent photofragmentation dynamics of a heavy-atom-containing bifunctional nitroimidazole radiosensitizer *Phys. Chem. Chem. Phys.* **26** 8879